



CHORUS

This is the accepted manuscript made available via CHORUS. The article has been published as:

Hard-X-Ray Spectroscopy with a Spectrographic Approach

Aleksandr I. Chumakov, Yuri Shvyd'ko, Ilya Sergueev, Dimitrios Bessas, and Rudolf Ruffer

Phys. Rev. Lett. **123**, 097402 — Published 29 August 2019

DOI: [10.1103/PhysRevLett.123.097402](https://doi.org/10.1103/PhysRevLett.123.097402)

Hard-x-ray spectroscopy with a spectrographic approach

Aleksandr I. Chumakov,^{1,*} Yuri Shvyd'ko,^{2,†} Ilya Sergueev,³ Dimitrios Bessas,¹ and Rudolf Ruffer¹

¹*ESRF – The European Synchrotron; Grenoble, France*

²*Advanced Photon Source, Argonne National Laboratory; Lemont, Illinois; United States of America*

³*Deutsches Elektronen Synchrotron; Hamburg, Germany*

Hard x-ray spectroscopy relies on a suite of modern techniques for studies of vibrational, electronic, and magnetic excitations in condensed matter. At present, the energy resolution of these techniques can be improved only by decreasing the spectral window of the involved optics — monochromators and analyzers — thereby, sacrificing the intensity. Here, we demonstrate hard x-ray spectroscopy with greatly improved energy resolution without narrowing the spectral window, by adapting principles of spectrographic imaging to the hard x-ray regime. Similar to classical Newton's prism, the hard x-ray spectrograph disperses different 'colors' — i.e., energies — of x-ray photons in space. Then, selecting each energy component with a slit ensures high energy resolution, whereas measuring x-ray spectra with all components of a broad spectral window keeps the intensity. We employ the principles of spectrographic imaging for phonon spectroscopy. Here the new approach revealed anomalous soft atomic dynamics in α -iron, a phenomenon which was not previously reported in literature. We argue that hard x-ray spectrographic imaging also could be a path to discovering new physics in studies of electronic and magnetic excitations.

PACS numbers: 07.85.Nc, 25.40.Ep, 63.20.-e, 76.80.+y

X-ray spectroscopy exploits a powerful set of tools to access new physics in studies of vibrational [1, 2], electronic [3, 4], and magnetic [5, 6] properties of solids. The best performance of these techniques is achieved in a delicate compromise between energy resolution and count rate. Improvements in each of these parameters are highly desirable: Better energy resolution is highly demanded [7–9] as it promises to open new physics, whereas higher intensity would greatly facilitate measurements. At present, however, the gain in quality — energy resolution — has been achieved in hard x-ray domain only by narrowing the spectral window of monochromators and analyzers and thereby sacrificing intensity.

A breakthrough solution to this problem would be to complement hard x-ray spectroscopies by principles of spectrographic imaging, widely used in a vast spectral range from infrared radiation to soft x rays. While a monochromator and analyzer work as narrow-band filters, cutting all radiation energies — i.e., 'colors' — but the desired one, a spectrograph keeps radiation components of all energies, dispersing the colors spatially. Consequently, the energy resolution is then provided by selecting distinct components in space, whereas the availability of all these components keeps the entire intensity.

For visible light, the concept of spectrographic imaging — dispersion of radiation components with various energies in space — is known since Newton's time [10]. For hard x rays, optical prisms and conventional diffraction gratings are not efficient. Nevertheless, the principles of angular dispersion of hard x rays are known [11–15], and the optical schemes of hard x-ray spectrographs have

been studied [13] and demonstrated [12]. They rely on the angular dispersion of x rays in Bragg diffraction by asymmetrically cut crystals [12–15]. Combined with focusing optics, this results in dispersing x rays of different energies in space [12, 13, 16, 17], localizing the narrowest energy bands in each spatial coordinate, and using the entire beam in all spatial coordinates in parallel, in order to preserve the total intensity.

In this study, we applied the principles of spectrographic imaging to phonon spectroscopy. Similar to previous suggestions [13, 17], we show that it also can be efficiently applied for studies of electronic and magnetic excitations. The implemented optical scheme can be adapted to any specific energy in a broad range of hard x rays, which is crucial for resonance inelastic scattering spectroscopies. Furthermore, it provides a large — many eV — scanning range, which is indispensable for studies of vibrational, electronic, and magnetic excitations. Applied to phonon spectroscopy, the hard x-ray spectrographic imaging reveals in this study anomalous soft atomic dynamics in α -iron, a phenomenon which was not previously reported in literature.

The study was performed at the Nuclear Resonance beamline [18] ID18 of the European Synchrotron Radiation Facility (ESRF). The principles of spectrographic imaging were applied for measurements of the density of phonon states by nuclear inelastic scattering [19] using 14.4125 keV photons corresponding to the energy of the nuclear resonance transition of the ^{57}Fe isotope. Figure 1a illustrates an integration of the spectrograph into the beamline layout. Figure 1b shows the optical scheme of the spectrograph. The dispersion is provided by the second and the third silicon crystals in the highly asymmetric (12 2 2) reflections. The second crystal provides negative angular dispersion $d\theta/dE$ of $-0.3 \mu\text{rad}/\text{meV}$. The third crystal inverts the sign of this contribution, in-

*Electronic address: chumakov@esrf.fr; Also at National Research Center "Kurchatov Institute", 123182 Moscow, Russia

†Electronic address: shvydko@anl.gov

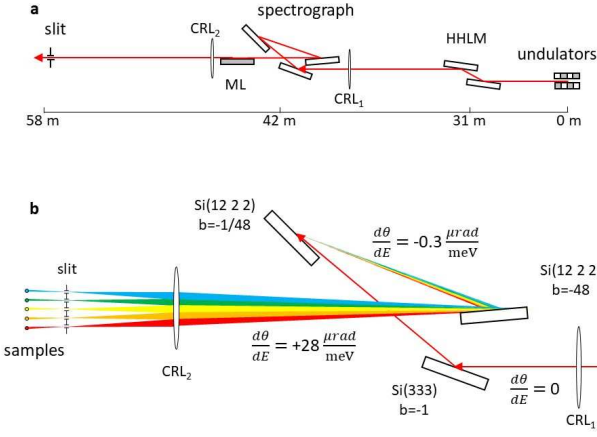


FIG. 1: The experimental setup. (a) The beamline layout with the indicated distances of the elements from the source. High-heat-load monochromator (HHLM); Compound refractive lenses (CRL); Multilayer mirror (ML). (b) Optical scheme of the spectrograph with the parameters of the optical elements and angular dispersion $d\theta/dE$ in various points of the scheme. Blue to red colours correspond to photons of highest to lowest energies, respectively.

increases it to $+14 \mu\text{rad}/\text{meV}$, and adds its own contribution of the same value, boosting the total dispersion to $+28 \mu\text{rad}/\text{meV}$. The multilayer mirror inverts the dispersion to $-28 \mu\text{rad}/\text{meV}$, proving finally higher-energy photons at lower vertical coordinate (Fig. 2a). The first silicon crystal is used to maintain the exit beam in the horizontal direction approximately, and the multilayer assures this precisely. The compound refractive lenses focus radiation components with different energies to different vertical coordinates of the slit, providing the spatial dispersion. More details of the optical scheme are discussed in Supplementary Material (SM) [20].

The described development of the angular dispersion $d\theta/dE$ (also called cumulative angular dispersion D_c) through the optical scheme is elaborated in Refs. [12–15]. For the given sequence of reflections, it is given by:

$$\frac{d\theta}{dE} \equiv D_c = D_3 + b_3 D_2 + b_3 b_2 D_1, \quad (1)$$

$$D_i = -\frac{(1 + b_i) \tan \theta_i}{E}, \quad (2)$$

where D_i , b_i , and θ_i are the angular dispersion, asymmetry factor, and Bragg angle of i -th crystal, respectively, and E is the x-ray energy. The asymmetry factor is defined as $b = -\sin \theta_{in} / \sin \theta_{out}$, with θ_{in} and θ_{out} the angles of the incident and exit beams, relative to the crystal surface, respectively. Note that for the first symmetric reflection $b_1 = -1$ and $D_1 = 0$. The energy resolution of the spectrograph ΔE is given by [12, 13, 16]:

$$\Delta E = \frac{\Delta S}{L} \frac{|b_c|}{D_c}, \quad (3)$$

$$b_c = b_1 b_2 b_3, \quad (4)$$

where ΔS is the effective source size, L is the distance from the source to the spectrograph, and b_c is the cumulative asymmetry coefficient. Using the parameters of the crystals and of the source listed in SM [20], one obtains from Eqs.(1-4) the expected dispersion rate $d\theta/dE = -29.5 \mu\text{rad}/\text{meV}$ and the expected energy resolution $\Delta E = 40 \mu\text{eV}$.

The key role in achieving the high dispersion and, therefore, ultra-high energy resolution belongs to the multi-crystal optical scheme [12, 13]. In comparison to a one-crystal setup [16], the current scheme increases the dispersion by a factor of two (eq.[1]). More importantly, it keeps the cumulative asymmetry coefficient b_c small (eq.[4]), improving altogether the energy resolution by nearly two orders of magnitude (eq.[3]).

Equation (3) shows that the energy resolution of the spectrograph is inversely proportional to the source-spectrograph distance L . In this study, this distance was limited to 42 m (Fig. 1a). At the upgraded Nuclear Resonance beamline ID18 of the ESRF, it could be increased to ~ 160 m, which should result in an energy resolution of $\sim 10 \mu\text{eV}$.

The angular dispersion and the energy resolution of the spectrograph were measured using the setup shown in Fig. 2a. The energy of x rays from the spectrograph was varied by simultaneous rotation of all three (Fig. 1)

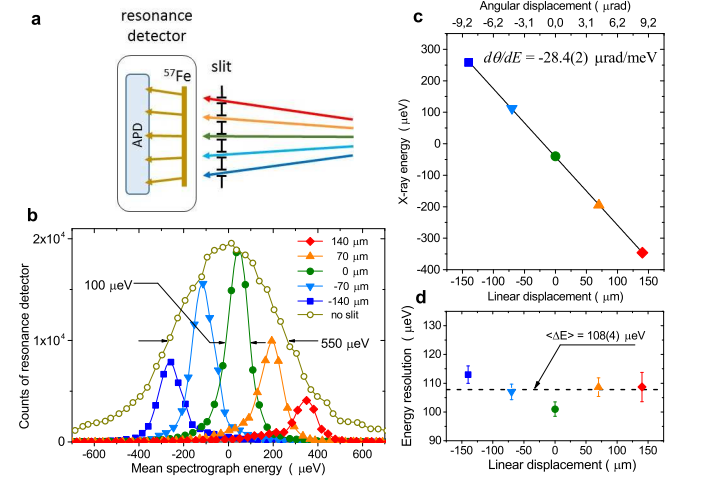


FIG. 2: The measurements of the energy resolution and of the angular dispersion. (a) The optical scheme. The ^{57}Fe foil and avalanche photo diode (APD) [51] function as a resonance detector with a bandwidth of $\sim 0.50 \mu\text{eV}$ (see SM [20]). (b) The x-ray intensity recorded by the resonance detector as the function of the mean energy of the spectrograph (see text) without the slit, and for five indicated vertical positions of a $20 \mu\text{m}$ -wide slit. (c, d) The energies (c) and the energy bandwidths (d) of the x-ray components selected by the slit at various vertical positions for the mean energy of the spectrograph at resonance. The values are obtained by fitting Lorentz curves to the data displayed in (b). The error bars are obtained from the fits. For (c), they are within the symbol size. The value and error bar of the angular dispersion are obtained by a linear fit (solid line) to the data displayed in (c). The dashed line in (d) shows the energy resolution averaged over five slit positions. Blue to red colours correspond to photons of highest to lowest energies, respectively.

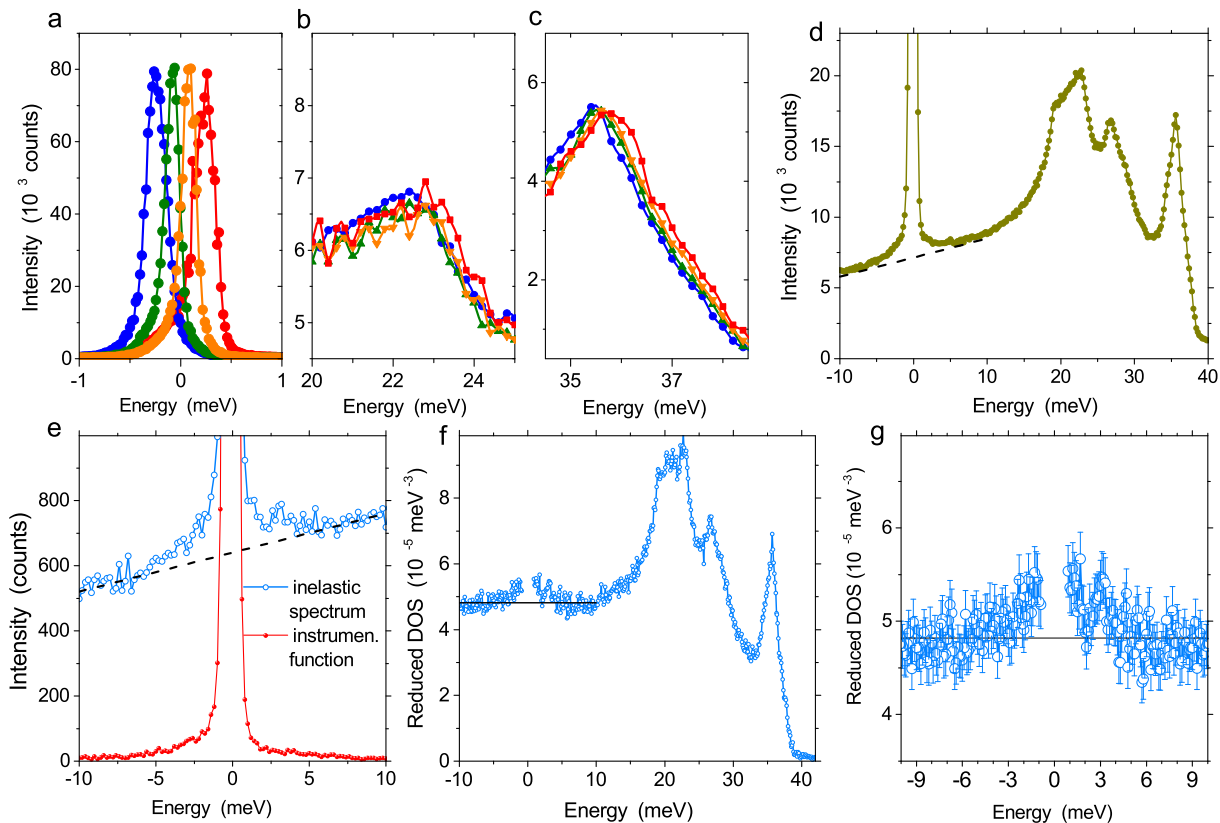


FIG. 3: (a-d) An example of phonon spectroscopy with the gain in quality — energy resolution — but without sacrificing quantity — intensity from a broad spectral window. (a-c) Various parts of the energy spectra of nuclear inelastic scattering measured in parallel with four identical foils of α -iron located at different vertical positions. The data are scaled to the same peak values to facilitate comparison. (d) The net spectrum obtained after the elimination of the relative shift between the spectra shown in (a-c) and adding them together (see text). (e) The inelastic spectrum and instrumental function measured for a single foil of α -iron. The data are scaled to the same peak value. The dashed line in (d, e) emphasizes the presence of the soft modes. (f) The reduced DOS $g(E)/E^2$, with the central part enlarged in (g). The data at positive and negative energies are derived from the corresponding parts of the inelastic spectrum shown in (e). The black horizontal line in (f, g) shows the Debye level — the expected contribution to the reduced DOS from the acoustic modes [20]. The error bars indicate the statistical uncertainty. Only those points are shown, where the systematic uncertainty related to the subtraction of the elastic peak is less than the symbol size.

silicon crystals [20]. The energies of the radiation components selected by the slit at five various vertical positions (successively, one after another) were determined using the resonance detector [20]. The detector and the slit act here as a position sensitive detector, and they are to be substituted by such a detector in future experiments [20].

Figure 2b shows the intensity of x rays recorded by the resonance detector as a function of the mean energy of the spectrograph, i.e., the energy of x rays on the optical axis, at zero vertical position of the slit. Without the slit, these measurements give the spectral window of the spectrograph. With a sufficiently small slit (in our case — $20 \mu\text{m}$, see SM [20]), the measurements give the energy resolution of the spectrograph. Figure 2b shows that the spectral window of the spectrograph is $550 \mu\text{eV}$, and the energy resolution is about $100 \mu\text{eV}$.

The energy and the bandwidth of the x-ray components selected by the slit at various vertical positions for a fixed mean energy of the spectrograph (see SM [20] for details) are shown in Figs. 2c and 2d, respectively. The angular dispersion rate $d\theta/dE = -28.4(2) \mu\text{rad}/\text{meV}$

is calculated from the slope of the photon energy plotted as a function of the vertical angle in Fig. 2c. The slight deviation from the expected value of $-29.5 \mu\text{rad}/\text{meV}$ can be attributed to a small (0.02 degree) miscut of the crystal surface.

The energy resolution of the spectrograph given by the bandwidth of the spectral components measured with the $20 \mu\text{m}$ slit is shown in Fig. 2d. It slightly varies over the vertical coordinates of the beam, from $101(3) \mu\text{eV}$ to $113(3) \mu\text{eV}$, with a mean value of $108(4) \mu\text{eV}$. This is larger than the expected value of $40 \mu\text{eV}$. The deviation could be caused by a small (2 mK) temperature inhomogeneity of the crystal surface, a slight ($\Delta d/d = 6 \times 10^{-9}$) inhomogeneity of the lattice constant, and/or a small ($\sim 30 \text{ nrad}$) bending of the atomic planes [20].

Figure 2 demonstrates that our approach may enable hard x-ray spectroscopy with an energy resolution of $\sim 100 \mu\text{eV}$ using all radiation components within the spectral window of $\sim 550 \mu\text{eV}$. The resolution of $\sim 100 \mu\text{eV}$ ($\sim 0.8 \text{ cm}^{-1}$) compares with the best resolution of Raman spectroscopy. Furthermore, it is about

an order of magnitude better than the typical resolution of presently employed hard x-ray inelastic scattering spectrometers [1, 2, 7]. For nuclear inelastic scattering, improving energy resolution is certainly easier as the method does not require energy analyzes and momentum resolution.

Figure 3 presents the application of the spectrograph for measurements of the density of phonon states of α -iron. The measurements were performed in parallel with four identical foils of α - ^{57}Fe , separated in the vertical coordinate with an increment of $\sim 70\ \mu\text{m}$ (see SM [20]). For a fixed mean energy of the spectrograph, they are illuminated by x rays of different energies (Fig. 2c). Accordingly, the measured spectra are shifted relative to each other, with the corresponding energy increment of $\sim 160\ \mu\text{eV}$ (Figs. 3a-3c). In data treatment, before adding the spectra, this relative shift is eliminated by centring all elastic peaks at zero energy. Figure 3d shows the obtained net spectrum of nuclear inelastic scattering in α -iron. It is measured with the high energy resolution while using the photons of the nearly entire spectral window of the spectrograph. The excellent $\sim 1\%$ statistical accuracy of the data has been reached in ~ 15 hours of measurements.

The noticeable tails of the elastic peak in the spectrum (Fig. 3d) suggest the presence of soft modes in α - ^{57}Fe , a phenomenon which was not previously reported in literature. The existence of such modes was indicated in our earlier measurements with lower energy resolution ($\sim 0.7\ \text{meV}$), but we were not able to confirm the effect unambiguously: with the lower resolution, the effect could be eliminated by slightly "enforced" subtraction of an elastic peak [20].

Revealing fine spectral features at small phonon energies requires precise comparison of the measured spectrum to the instrumental function of the spectrograph. For measurements with several samples, this would require a position-sensitive detector for nuclear forward scattering [20]. Because this instrumentation is not yet available, we repeated the measurements with a single foil of α - ^{57}Fe , recording simultaneously the spectrum of nuclear inelastic scattering and the instrumental function [20]. The presence of the additional vibrational modes, noticeably more pronounced than the tails of the instrumental function, is seen already in the raw experimental data (Fig. 3e). Figures 3f-3g show the derived reduced density of the phonon state (DOS) $g(E)/E^2$. The presence of the anomalous soft modes above the level of acoustic modes, indicated by the straight horizontal line, is unambiguous.

Additional experimental data presented and discussed in SM [20] show that these modes cannot be attributed to possible imperfections as impurities, grain boundaries, dislocations, texture, and magnetic domain walls. They also are not an experimental artifact, because measurements of other systems do not show this feature [20].

In Supplementary Materials [20], we analyse several possible origins of the observed anomaly: (i) nano-

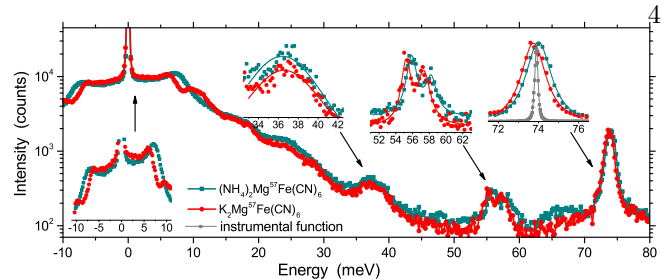


FIG. 4: Example of simultaneous spectroscopy of different hexacyanoferrates samples: $\text{K}_2\text{Mg}^{57}\text{Fe}(\text{CN})_6$ and $(\text{NH}_4)_2\text{Mg}^{57}\text{Fe}(\text{CN})_6$. The spectra are corrected for the relative energy shift caused by different sample positions (see text). The inserts emphasize the relative energies of the acoustic and optical modes and show the instrumental function of the spectrograph for comparison. The solid lines are to guide the eye.

structured inclusions, (ii) force-constant disorder [52], (iii) positive dispersion of acoustic modes, (iv) anharmonic effects [53], and (v) magneto-elastic waves [54]. The first two options seem to be not compatible with our experimental data and material properties. The model of positive dispersion appears to be not in agreement with the results of neutron studies [55]. Attributing the effect to anharmonicity is compatible with its temperature dependence [20].

The above example of the spectroscopy with several identical samples measured simultaneously demonstrates the key advantage of the approach: achieving ultra-high energy resolution while utilizing full intensity of a broad spectral window. Alternatively, one may also consider simultaneous measurements of different samples. In this case, the availability of ultra-high energy resolution and several beams enable precise studies of several systems simultaneously, eliminating systematic errors in the relative energies of their vibrational modes by measurements of several samples in parallel.

Figure 4 shows the spectra of nuclear inelastic scattering in $\text{K}_2\text{Mg}^{57}\text{Fe}(\text{CN})_6$ and $(\text{NH}_4)_2\text{Mg}^{57}\text{Fe}(\text{CN})_6$ hexacyanoferrates measured simultaneously. The samples reveal rather different acoustic modes, fairly identical optical modes at 37 meV, and slightly different optical modes at 55, 57, and 74 meV. The high energy resolution enables the precise determination of these tiniest differences, whereas the simultaneous measurements exclude systematic errors. For example, the relative shift of $254\ \mu\text{eV}$ between the $\sim 74\ \text{meV}$ optical modes of two hexacyanoferrates is determined with an accuracy of $19\ \mu\text{eV}$ ($\sim 0.15\ \text{cm}^{-1}$). This approach would be especially beneficial for studies of proteins dynamics [56].

Figure 4 also demonstrates that the energy widths of the optical phonons in the density of states are no longer limited by the energy resolution: they are much larger than the width of the instrumental function. This can be attributed to a noticeable dispersion of the optical modes in the space of momentum transfer and/or a measurable lifetime of the phonons.

Finally, we note that the extension of the principles of spectrographic imaging to the hard x-ray regime may

have a very wide range of applications. For phonon studies, we demonstrated the improvement in the energy resolution while using radiation in a broad spectral window. For other applications, one can also target the opposite goal: to boost the intensity without sacrificing the energy resolution. Here, using nearly the same scheme, one may keep an energy resolution of ~ 0.6 meV while increasing a spectral window to ~ 2 meV (see SM [20]).

Furthermore, the same approach also can be extended to studies of electronic and magnetic excitations, e.g., in topical scientific cases tackled by Resonance Inelastic X-ray Scattering at Ir-L3 and Os-L3 absorption edges [57, 58]. For studies of magnetic excitations, higher energy resolution is in real need [8, 9], and here our approach may ensure a ~ 1 -2 meV resolution and a ~ 10 meV spectral window [20]. For studies of electronic excitations, where the energy resolution is normally not an issue, it may offer a ~ 11 meV resolution and a ~ 160 meV spectral window [20]. For Cu-K edge, a similar approach may offer 1 meV resolution and 85 meV spectral window [13]. The discussed schemes can be used both for monochromator and/or analyzer branches of inelastic spectrometers [17].

In summary, we applied the principles of spectrographic imaging to the hard x-ray regime and demonstrated phonon spectroscopy with the tremendously improved energy resolution while preserving intensity from

the broad spectral window. For nuclear inelastic scattering, this approach provided an energy resolution of ~ 100 μ eV, which is about an order of magnitude better than the typical resolution of presently employed hard x-ray inelastic scattering spectrometers [1, 2, 7]. Certainly, here it is easier to achieve as the method does not require energy analyzers and momentum resolution.

Applied to studies of phonons, this approach revealed anomalous soft atomic dynamics in α -iron, a phenomenon which was not previously reported in literature. We expect that it may also reveal new phenomena in the physics of electronic and magnetic excitations.

The authors are grateful to Jean-Pierre Vassalli, Benoit Picut, Christian Morawe, Amparo Vivo, Francois Perrin, and Ray Barrett for manufacturing and characterizing the silicon crystals and the multilayer mirror, to Alexey Bosak for a loan of an α -iron single crystal and fruitful discussions, and to Jean-Philippe Celse for technical help. AIC thanks Alfred Q.R. Baron for the idea to look more carefully at the acoustic modes of α -iron; Christoph Sahle and Marco Moretti for discussion on Resonance Inelastic X-ray Scattering; and Giulio Monaco, Federico Caporaletti, and Giacomo Baldi for discussion on the effects of anharmonicity. Work at Argonne National Laboratory was supported by the U.S. Department of Energy, Office of Science, under Contract No. DE-AC02-06CH11357.

-
- [1] D. J. Voneshen, K. Refson, E. Borissenko, M. Krisch, A. Bosak, A. Piovano, E. Enderle, M. Gutmann, M. Hoesch, M. Roger, L. Gannon, A. T. Boothroyd, S. Uthayakumar, D. G. Porter, and J. P. Goff, *Nature Materials* **12**, 1028 (2013).
- [2] M. Le Tacon, A. Bosak, S. M. Souliou, G. Dellea, T. Loew, R. Heid, K.-P. Bohnen, G. Ghiringhelli, M. Krisch, and B. Keimer, *Nature Physics* **10**, 52 (2014).
- [3] J. Schlappa, K. Wohlfeld, K. J. Zhou, M. Mourigal, M. W. Haverkort, V. N. Strocov, L. Hozoi, C. Monney, S. Nishimoto, S. Singh, A. Revcolevschi, J.-S. Caux, L. Patthey, H. M. Rønnow, J. van den Brink, and T. Schmitt, *Nature* **485**, 84 (2012).
- [4] Y. Y. Peng, R. Fumagalli, Y. Ding, M. Minola, S. Caprara, D. Betto, M. Bluschke, G. M. De Luca, K. Kummer, E. Lefrançois, M. Salluzzo, H. Suzuki, M. Le Tacon, X. J. Zhou, N. B. Brookes, B. Keimer, L. Braicovich, M. Grilli, and G. Ghiringhelli, *Nature Materials* **17**, 697 (2018).
- [5] M. Le Tacon, G. Ghiringhelli, J. Chaloupka, M. Moretti Sala, V. Hinkov, M. W. Haverkort, M. Minola, M. Bakr, K. J. Zhou, S. Blanco-Canosa, C. Monney, Y. T. Song, G. L. Sun, C. T. Lin, G. M. De Luca, M. Salluzzo, G. Khaliullin, T. Schmitt, L. Braicovich, and B. Keimer, *Nature Physics* **7**, 725 (2011).
- [6] M. P. M. Dean, G. Dellea, R. S. Springell, F. Yakhov-Harris, K. Kummer, N. B. Brookes, X. Liu, Y.-J. Sun, J. Strle, T. Schmitt, L. Braicovich, G. Ghiringhelli, I. Božović, and J. P. Hill, *Nature Materials* **12**, 1119 (2013).
- [7] A. Q. R. Baron. High-Resolution Inelastic X-Ray Scattering I: Context, Spectrometers, Samples, and Superconductors. In: *Synchrotron Light Sources and Free-Electron Lasers*. Jaeschke E., Khan S., Schneider J., Hastings J. (eds), Springer, Cham, (2015).
- [8] Y. Shvyd'ko, S. Stoupin, D. Shu, S. P. Collins, K. Mundboth, J. Sutter, and M. Tolkieln, *Nature Communications*, **5**, 4219 (2014).
- [9] J. Kim, D. Casa, A. Said, R. Krakora, B. J. Kim, E. Kasman, X. Huang, and T. Gog, *Scientific Reports*, **8**, 1958 (2018).
- [10] I. Newton, *Opticks*. London: Royal Society, (1704).
- [11] T. Matsushita and U. Kaminaga, *Journal of Applied Crystallography* **13**, 472 (1980).
- [12] Y. Shvyd'ko, S. Stoupin, K. Mundboth, and J. Kim, *Phys. Rev. A* **87**, 043835 (2013).
- [13] Y. Shvyd'ko, *Phys. Rev. A* **91**, 053817 (2015).
- [14] Y. Shvyd'ko, *X-Ray Optics — High-Energy-Resolution Applications*, vol. **98** of *Optical Sciences* (Springer, Berlin, 2004).
- [15] Y. V. Shvyd'ko, M. Lerche, U. Kuetgens, H. D. Rüter, A. Alatas, and J. Zhao, *Phys. Rev. Lett.* **97**, 235502, (2006).
- [16] V. G. Kohn, A. I. Chumakov, and R. Ruffer, *J. Synchrotron Radiation* **16**, 635 (2009).
- [17] Yu. Shvyd'ko, *Phys. Rev. Lett.* **116**, 080801 (2016).
- [18] R. Ruffer and A. I. Chumakov, *Hyperfine Interactions* **97/98**, 589 (1996).
- [19] M. Seto, Y. Yoda, S. Kikuta, X. W. Zhang, and M. Ando, *Phys. Rev. Lett.* **74**, 3828 (1995).

- [20] See Supplemental Material [url] for description of samples, experiment, and data analysis, which includes Refs. [21–50].
- [21] J. B. Hastings, D. P. Siddons, U. van Bürck, R. Hollatz, and U. Bergmann, *Phys. Rev. Lett.* **66**, 770773 (1991).
- [22] A. I. Chumakov, I. Sergeev, J.-P. Celse, R. Ruffer, M. Lesourd, L. Zhang and M. Sanchez del Rio, *J. Synchrotron Rad.* **21**, 315324 (2014).
- [23] Yu. V. Shvyd'ko, M. Lerche, J. Jäschke, M. Lucht, E. Gerdau, M. Gerken, H. D. Rüter, H.-C. Wille, P. Becker, E. E. Alp, W. Sturhahn, J. Sutter, and T. S. Toellner, *Phys. Rev. Lett.* **85**, 495 (2000).
- [24] A. I. Chumakov, R. Ruffer, O. Leupold, A. Barla, H. Thiess, T. Asthalter, B. P. Doyle, A. Snigirev, A. Q. R. Baron, *Appl. Phys. Lett.* **77**, 31 (2000).
- [25] E. Gerdau, H. de Waard (Eds.), *Nuclear Resonant Scattering of Synchrotron Radiation, Hyperfine Interactions*, vol. **123125**, Baltzer Science Publishers (1999/2000).
- [26] R. Röhlsberger. *Nuclear Condensed Matter Physics with Synchrotron Radiation Basic Principles, Methodology and Applications*. Springer Tracts in Modern Physics, vol. **208**, Springer Publishers (2004).
- [27] P. Fajardo, A. Q. R. Baron, H. Dautet, M. Davies, P. Fischer, P. Göttlicher, H. Graafsma, C. Hervé, R. Ruffer, and C. Thil, *Journal of Physics : Conference Series* **425**, 062005 (2013).
- [28] S. Kishimoto, H. Yonemura, S. Adachi, S. Shimazaki, M. Ikeno, M. Saito, T. Taniguchi and M. Tanaka, *Journal of Physics: Conference Series*, **425**, 062007 (2013).
- [29] T. Masuda, S. Okubo, H. Hara, T. Hiraki, S. Kitao, Y. Miyamoto, K. Okai, R. Ozaki, N. Sasao, M. Seto, S. Uetake, A. Yamaguchi, Y. Yoda, A. Yoshimi, and K. Yoshimura, *Review of Scientific Instruments* **88**, 063105 (2017).
- [30] A. I. Chumakov and W. Sturhahn, **123/124**, 781 (1999).
- [31] A. I. Chumakov, R. Ruffer, *Hyperfine Interactions* **113**, 59 (1998).
- [32] V. G. Kohn and A. I. Chumakov, *Hyperfine Interactions* **125**, 205 (2000).
- [33] A. Sjölander, *Arkiv for Fysik* **14**, 315 (1958).
- [34] B. Roldan Cuenya, L. K. Ono, J. R. Croy, K. Paredis, A. Kara, H. Heinrich, J. Zhao, E. E. Alp, A. T. DelaRiva, A. Datye, E. A. Stach, and W. Keune, *Physical Review B*, **86**, 165406 (2012).
- [35] W. Schirmacher, G. Diezemann, and C. Ganter, *Physical Review Letters*, **81**, 136 (1998).
- [36] J. Ramakrishnan, R. Boehler, G. H. Higgins, and G. C. Kennedy, *Journal of Geophysical Research*, **83**, 3535 (1978).
- [37] H.-K. Mao, W. A. Bassett, and T. Takahashi, *Journal of Applied Physics*, **38**, 272 (1967).
- [38] K. E. Metzloff, H. W. Kwon, L. Y. Fang, C. R. Loper, in *Service Modulus: A Method for Accurate Determination of Young's Modulus and Yield Strength in Ductile Iron (96-53)*, American Foundrymen's Society, 1997.
- [39] Q. Wei, C. McCammon, and S. A. Gilder, *Geochemistry, Geophysics, Geosystems*, **18**. <https://doi.org/10.1002/2017GC007143>
- [40] J. Zarestky and C. Stassis, *Phys. Rev. B* **35**, 4500 (1987).
- [41] L. Mauger, M. S. Lucas, J. A. Muñoz, S. J. Tracy, M. Kresch, Y. Xiao, P. Chow, and B. Fultz, *Physical Review B* **90**, 064303 (2014).
- [42] F. Körmann, B. Grabowski, B. Dutta, T. Hickel, L. Mauger, B. Fultz, and J. Neugebauer, *Physical Review Letters*, **113**, 165503 (2014).
- [43] M. F. Collins, V. J. Minkiewicz, R. Nathans, L. Passell, and G. Shirane, *Phys. Rev.* **179**, 417 (1969).
- [44] H. R. Schober and P. H. Dederichs, in: *Phonon States of Elements. Electron States and Fermi Surfaces of Alloys*, LandoltBörnstein, Vol. III/13a, eds. K.-H. Hellwege and J. L. Olsen (Springer, Berlin, 1981) p. 56.
- [45] V. N. Strocov, *Journal of Synchrotron Radiation*, **17**, 103 (2010).
- [46] K. Achterhold, C. Keppler, A. Ostermann, U. van Bürck, W. Sturhahn, E. E. Alp, and F. G. Parak, *Phys. Rev. E* **65**, 051916 (2002).
- [47] M. Y. Hu, W. Sturhahn, T. S. Toellner, P. D. Mannheim, D. E. Brown, J. Zhao, and E. E. Alp, *Phys. Rev. B* **67**, 094304 (2003).
- [48] A. I. Chumakov, A. Bosak, and R. Ruffer, *Phys. Rev. B* **80**, 094303 (2009).
- [49] D. J. Dever, *J. Appl. Phys.* **43**, 3293 (1972).
- [50] C. A. Rotter and C. Smith, *J. Phys. Chem. Solids* **27**, 267 (1996).
- [51] A. Q. R. Baron, *Hyperfine Interact.*, **125**, 29 (2000).
- [52] W. Schirmacher, G. Ruocco, and T. Scopigno, *Phys. Rev. Lett.* **98**, 025501 (2007).
- [53] J. Scheipers and W. Schirmacher, *Z. Phys. B* **103** 547 (1997).
- [54] A. I. Akhiezer, V. G. Bar'yakhtar, S. V. Peletminskii. *Spin waves* (North-Holland Publishing Company, Amsterdam, 1968).
- [55] J. Neuhaus, M. Leitner, K. Nicolaus, W. Petry, B. Hennion, and A. Hiess, *Phys. Rev. B* **89**, 184302 (2014).
- [56] E. J. Reijerse, C. C. Pham, V. Pelmeshnikov, R. Gilbert-Wilson, A. Adamska-Venkatesh, J. F. Siebel, L. B. Gee, Y. Yoda, K. Tamasaku, W. Lubitz, T. B. Rauchfuss, S. P. Cramer, *J. Am. Chem. Soc.*, **139**, 4306 (2017).
- [57] T. Takayama, A. Yaresko, A. Matsumoto, J. Nuss, K. Ishii, M. Yoshida, J. Mizuki, and H. Takagi, *Scientific Reports*, **4**, 6818 (2014).
- [58] S. Calder, J. G. Vale, N. A. Bogdanov, X. Liu, C. Donnerer, M. H. Upton, D. Casa, A. H. Said, M. D. Lumsden, Z. Zhao, J.-Q. Yan, D. Mandrus, S. Nishimoto, J. van den Brink, J. P. Hill, D. F. McMorrow, and A. D. Christianson, *Nat. Commun.* **7**, 11651 (2016).